Biomaterials 34 (2013) 10217–10227

Contents lists available at ScienceDirect

Biomaterials

journal homepage: www.elsevier.com/locate/biomaterials

The performance of thiol-terminated PEG-paclitaxel-conjugated gold nanoparticles

Ya Ding [a, *], Ying-Ying Zhou [a], Huan Chen [b], Dong-Dong Geng [a], Dong-Yan Wu [a], Jin Hong [a, c], Wen-Bin Shen [a], Tai-Jun Hang [a], Can Zhang [a]

[a] Key Laboratory of Drug Quality Control and Pharmacovigilance, China Pharmaceutical University, Ministry of Education, Nanjing 210009, China
[b] Department of Biochemistry, School of Life Science and Technology, China Pharmaceutical University, Nanjing 210009, China
[c] State Key Laboratory of Coordination Chemistry, Coordination Chemistry Institute, Nanjing University, Nanjing 210093, China

ARTICLE INFO

Article history:
Received 11 August 2013
Accepted 2 September 2013
Available online 20 September 2013

Keywords:
Paclitaxel-conjugated gold nanoparticles
Double simultaneous stimulation
Target selection
Drug release
Tumor therapeutic efficacy
Overall performance improvement

ABSTRACT

A series of thiol-terminated polyethylene glycol (PEG)-paclitaxel (PTX) derivatives are designed and synthesized to fabricate PTX-conjugated gold nanoparticles (PTX@GNPs) and improve their overall performance. By extending the molecular weight of PEG from 400 to 1000 Da, the optimized water solubility of the conjugate reaches 184 mg/mL, equal to 4.6×10^5 times that of PTX alone (0.4 μg/mL). High drug loading is obtained by eliminating the steric hindrance between PTX molecules on the surface of GNPs. The gold conjugate shows double simultaneous stimulation-induced drug release behavior in the presence of both esterase and high concentrations of glutathione. The synergic release characteristics of this conjugate results in significant performance improvements, including prolonged circulation due to high stability in vivo, targeted release of PTX inside tumor cells, and increased tumor cell killing efficiency. Improving the in vitro properties of the conjugate not only significantly enhances its therapeutic efficacy in a murine liver cancer model, but also allows drug-conjugated gold nanoparticles to be used as a promising nanoprodrug system in the cancer therapeutics.

1. Introduction

Many hydrophobic antitumor substances have limited clinical applications due to their low solubility, fragile stability, and the serious side effects caused by nonspecific biodistribution in the body. Due to its effective, broad-spectrum chemotherapeutic activity and its notorious poor water solubility, Paclitaxel (PTX)-based drug delivery systems (DDSs) have attracted tremendous attention for the treatment of cancer. Recently, a variety of PTX formulations, including prodrugs, micelles, liposomes, solid lipid nanoparticles, dendrimers, nanohydrogels, and drug-eluting stents, have been reviewed to describe the important role of pharmaceutical nanotechnology for the development of PTX-based DDSs [1]. Among them, gold nanoparticle (GNP)-based DDS [2], especially monolayer protected GNPs, is considered to be a promising prodrug strategy to overcome the practical application problems of PTX in the nanoscale [3,4]. This strategy has also been applied to a number of other drugs, including Ciprofloxacin [5], Doxorubicin [6–9], Curcumin [10], and Chloroquine [11].

As opposed to encapsulating drug molecules within the hydrophobic core of carriers with hydrophilic shells [12–14], monolayer protected GNPs are constructed by covalently conjugating drug molecules to the surface of water-soluble GNPs. The tunable size and high surface-to-volume ratio of GNPs allow surface functionalization with a large number of active molecules for specific targeting and drug payloads [15–21]. Moreover, the conjugating reactivity, chemical inertness, and low innate cytotoxicity of GNPs are desirable properties for their potential use as a drug carrier with high biocompatibility [22]. However, there are still several problems that must be overcome prior to the practical application of drug-conjugated GNP systems, especially for paclitaxel.

To increase the hydrophilicity and targeting capability of PTX, tumor necrosis factor (TNF), thiolated polyethylene glycol (PEG), and thiolated PTX were conjugated to the surface of GNPs at the same time as PTX to target and treat solid tumors [2,4]. However, the simultaneous surface modification of other ligands competitively occupied the bonding sites that anchor PTX to the gold surface, decreasing the PTX loading capacity of these

* Corresponding author. Tel./fax: +86 25 83271171.
E-mail address: ayanju@163.com (Y. Ding).

0142-9612/$ – see front matter © 2013 Elsevier Ltd. All rights reserved.
http://dx.doi.org/10.1016/j.biomaterials.2013.09.008

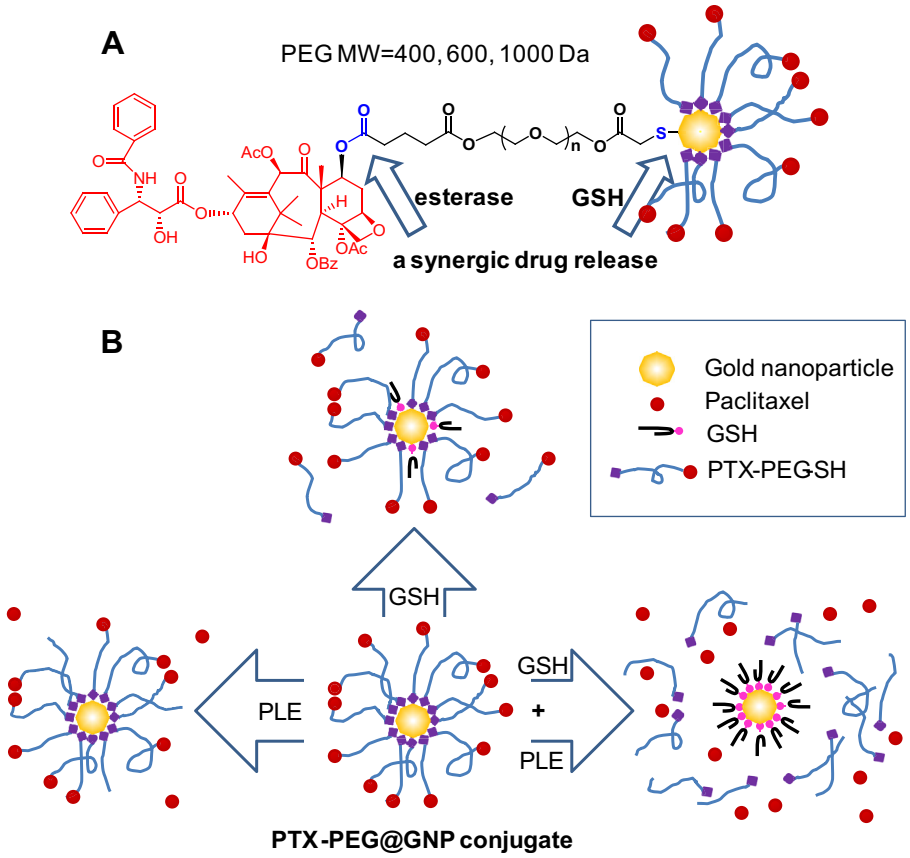

Fig. 1. Schematic illustration of (A) the chemical structure of PTX-PEG@GNP conjugates (PEG MW = 400, 600, and 1000 Da), and (B) the drug release profiles of PTX-PEG$_{1000}$@GNPs in response to high GSH concentrations and pig liver esterase.

nanoconjugates and making the quantitative study of the system difficult. Thus, to accurately define the number of drug molecules anchored to the GNP surface, PTX molecules were coupled to phenol-terminated gold nanocrystals (approximately 2 nm) via a hexaethylene glycol linker [23]. The number of PTX molecule conjugated to the gold surface was ~70 molecules per nanoparticle, and the drug loading capacity (DLC) was 6.2% (according to the equation: DLC% = the weight of drug in conjugate/the weight of conjugate × 100%). In this case, the water solubility and DLC of the system was not suitable for biological delivery. More recently, DNA linkers have been employed to covalently attach PTX to GNPs, increasing its internalization in a variety of cell types. The conjugated PTX-DNA@GNPs exhibited more than a 50-fold increase in solubility compared to the unconjugated drug (0.4 μg/mL) [24], reaching an equivalent PTX concentration of 21.35 μg/mL [25]. Furthermore, introducing a phosphate joining unit between the connecting arm (tetraethylene glycol-SH) and the PTX molecule increased the liberation rate of PTX in the presence of phosphodiesterase [26]. These results suggest that the hydrophilicity of the spacer between PTX and the gold nanoparticle and the connecting group between PTX and the spacer greatly influenced the solubility and drug release behavior of gold conjugates. However, the solubility and drug loading capacity of PTX-conjugated gold nanoparticles are far less than those reported for PTX encapsulated by polymeric micelles (solubility: 1–2.5 mg/mL, DLC: 15–40%) [27–29]. Therefore, based on these reports, a nanoparticle-based drug delivery system has not yet been shown to provide the advantages one might expect. Thus, improving their overall performance, including water solubility, drug loading capacity, stimulant-induced drug release inside tumor cells, and tumor treatment efficacy, remains challenging.

In the present work, we design and synthesize a series of mercapto group-terminated PEG-PTX ligands to fabricate GNP-conjugated PTX nanoparticles (shown in Fig. 1A) for overcoming the problems associated with nanoparticle-based DDSs. In contrast to previous studies, the chemical structures of our therapeutic ligands are designed rationally with the following aspects: (1) the therapeutic ligand contains a thiol group at the end of one terminal, allowing one-pot preparation using the ligand exchange method; (2) the oligoethylene glycol linkers are extended to polyethylene glycol with molecular weights of 400, 600, and 1000 Da to optimize the conjugate solubility in water; (3) the double simultaneous stimulation-triggered drug release characteristics (Fig. 1B) give the prodrug high stability in vivo and selective drug targeting inside tumor cells. To confirm the overall performance improvement of thiol-terminated PEG-paclitaxel-conjugated gold nanoparticles, the detailed characterization of the physicochemical and pharmaceutical properties for gold conjugates has been carried out. And then, their tumor treatment efficacy in the tumor bearing mouse models is systematically investigated and compared to the commercial PTX formulation (Taxol®).

2. Materials and methods

2.1. Materials

Hydrogen tetrachloroaurate hydrate ($HAuCl_4 \cdot 3H_2O$) was obtained from the Shanghai Chemical Regent Company (China). Polyethylene glycol (molecular weights of 400, 600, and 1000 Da), N, N′-dicyclohexylcarbodiimide (DCC), and 4-

dimethylamiopryidine (DMAP) were obtained from Sigma–Aldrich (USA). Thioctic acid (TA, 99%) was purchased from Nanjing Zelang Pharmaceutical Technology (China). Paclitaxel was obtained from Yew Pharmaceutical Co (Jiangsu, China). Pig liver esterase (PLE) was purchased from Sigma–Aldrich (USA). Unless otherwise stated, all starting materials were obtained from commercial suppliers and were used without further purification. Solvents were dried using standard procedures. All aqueous solutions were prepared using deionized water (>18 MΩ, Purelab Classic Corp., USA).

2.2. Preparation of citrate-protected gold nanoparticles

Citrate-protected gold nanoparticles were synthesized in a single-phase system [30,31] by filtering sub-boiling water through a microporous membrane with an aperture of 0.22 μm. All glassware was cleaned in a bath of freshly prepared aqua regia and rinsed thoroughly with deionized water prior to use. Hydrogen tetrachloroaurate (III) trihydrate (0.615 mL, 0.02 g/mL) and solid sodium citrate (50 mg, 1.3 mmol) were dissolved in 50 mL of triply distilled H_2O. A freshly prepared and cooled aqueous solution of sodium borohydride (1.2 mL, 0.1 M) was added to the reaction solution, resulting in an immediate color change to pink. After vigorous stirring for 30 min, the resulting solution appeared as a burgundy-red colloidal dispersion of gold.

2.3. Synthesis of therapeutic ligands (PTX-PEG$_{400,600,1000}$-SH)

The synthesis of PTX-PEG$_{1000}$-SH ligand was described in the Supporting Information as an example of the method used to synthesize all of the PTX-PEG-SH ligands. The ^{1}H and ^{13}C NMR data and FT-IR for the PTX-PEG$_{400,600,1000}$-SH ligands, as well as the NMR spectra for all the intermediates and final product of PTX-PEG$_{1000}$-SH are also presented in the Supporting Information.

2.4. Preparation of PTX-PEG@GNP conjugates

PTX-PEG-SH (0.28 mmol, PEG MW of 400, 600, and 1000 Da, respectively) was dissolved in 4 mL of methanol. Citrate-protected GNPs (3 mL) were added to the solution of PTX-PEG-SH, and the mixture was stirred for 1 h to obtain the gold conjugate solution. The gold conjugate solution was then aged overnight and dialyzed in a fresh deionized water solution for 72 h (molecular weight cut off (MWCO) = 7500). After freeze drying, the resulting deep orange syrupy substance was purified by gel separation chromatography using a Sephadex (G-25) gel column as the stationary phase and methanol: H_2O (30:70 v/v) as the mobile phase. The purified PTX-PEG$_{400,\ 600,\ 1000}$@GNP conjugates were characterized by Fourier transform infrared spectroscopy (FT-IR),Nuclear magnetic resonance (NMR), Ultraviolet–visible (UV–Vis) spectroscopy, thermogravimetric analysis (TGA), transmission electron microscopy (TEM), and dynamic light scattering (DLS).

2.5. Characterization

The chemical structures of the organic ligands in KBr discs were determined using a Tensor-27 Fourier IR spectrometer (Bruker, USA) equipped with a liquid nitrogen cooled mercury cadmium telluride (MCT) detector. ^{1}H and ^{13}C NMR spectra were recorded on a Bruker (AVACE) AV-500 spectrometer. Chemical shifts (δ) are listed in parts per million (ppm), using tetramethylsilane as an internal reference. UV–Vis spectra were measured with a UV-2401 PC UV/Vis spectrophotometer (Shimadzu, USA). The diameter, dispersity, and Zeta potentials of the conjugates were measured using a Zetasizer 3000HS instrument (Malvern Instruments, Malvern, UK) with 633 nm He–Ne lasers at 25 °C, while the lyophilized powder was reconstituted with double distilled water. A single drop of each solution was deposited on a TEM grid and allowed to air dry. All gold nanoparticle samples and conjugates were imaged using a JEM-200CX TEM (JEOL) with an acceleration voltage of 200 kV. TGA was performed using a thermal gravimetric analyzer (TG 209 F1, Netzsch, Germany).

Analytical reverse-phase high performance liquid chromatography (RP-HPLC) was performed using an Agilent 1100 series with a Diamonsil® C18 reversed-phase chromatography column (250 × 4.6 mm) and a UV detector set at 227 nm. A mobile phase of methanol/water (75/25, v/v) was used, and the flow rate was set at 1 mL/min (30 °C).

2.6. Stability studies

For stability analysis, PTX-PEG$_{1000}$@GNP conjugates were incubated at 37 °C under the following conditions: 0.03 M PBS at pH 7.4; pH 5.5, lowered by the addition of 1 mol/L HCl; higher ionic strength of 0.2 M PBS at pH 7.4; and in the presence of serum (at pH 7.4 in 0.03 M PBS solution with 2% serum). Absorbance of the conjugates at 520 nm was monitored at the indicated time points.

2.7. In vitro drug release

The release of PTX and PTX-PEG-SH ligands from conjugates was investigated by dialysis. The PTX-PEG$_{1000}$@GNPs (25 mg) containing 9.13 mg PTX were dissolved in phosphate-buffered saline (PBS, 2 mL) at pH 7.4 and placed in a dialysis bag (MWCO = 7500). To investigate drug release behavior in the presence of glutathione (GSH) or/and PLE, the above PBS solution containing Tween 80 (0.1%, w/v) was employed as the release medium. GSH concentrations in the release medium were set at 2 μM (extracellular level) and 10 mM (intracellular level) [32], and PLE containing 20 units was added. The PBS system was stirred at 150 rpm at 37 °C. At predetermined time intervals, 200 μL aliquots of release medium were withdrawn, and the same volume of fresh medium was added. The in vitro release behavior of the PTX-PEG$_{1000}$@GNPs, including the release of both the PTX-PEG$_{1000}$-SH ligand and PTX molecule, was measured by RP-HPLC analysis. All assays were performed in triplicate.

2.8. Cell culture

The human hepatocellular liver carcinoma cell line, HepG2, was purchased from the China Center for Type Culture Collection (Shanghai, China). For cytotoxicity assays, cells were seeded in a 96-well plate (1×10^4/well) using Dulbecco's modified Eagle's medium (DMEM) with 10% fetal bovine serum (FBS), and the plates were incubated at 37 °C in humidified atmosphere with 5% CO_2 for 24 h until they reached 80% confluence.

2.9. Cytotoxicity

HepG2 cells were incubated in growth medium with 3% FBS containing different concentrations of PTX-PEG$_{1000}$@GNPs, PTX-PEG$_{1000}$-SH ligand, and free PTX for 48 h. The cells were then washed twice with 200 μL of PBS and incubated in a growth medium containing 1 mg/mL 3-(4,5-dimethylthiazol-2-yl)-2,5-diphenyl-tetrazoliumbromide (MTT) (Sigma) for an additional 4 h at 37 °C. The medium was aspirated, and the MTT-formazan generated by living cells was dissolved in 150 μL of DMSO. The absorbance at 490 nm was measured in each well using a microplate reader (Bio-rad). The cell viability (%) was determined by comparing the absorbance at 490 nm with control wells containing only cell culture medium. Data are presented as the average ± SD ($n = 5$). The concentration of paclitaxel that inhibited 50% cell growth compared with untreated cells (IC_{50}) was defined by curve fitting (LOGIT method) using SPSS software. Each experiment was repeated three times.

2.10. Cellular uptake studies

HepG2 cells were seeded in 6-well plates at a density of 5×10^5 cells per well and incubated for 24 h to reach 80% confluence. The cells were then incubated for an additional 4 h or 8 h with PTX-PEG$_{1000}$@GNPs at a PTX dose of 2 μg/mL. Subsequently, excess media was removed, and the cells were washed with PBS, trypsinized and centrifuged. The cell pellets were fixed in a 0.1 M PBS solution containing 2.5% glutaraldehyde for 4 h, rinsed with 0.1 M PBS solution, post-fixed in 1% osmic acid, dehydrated through an acetone series and embedded in Epon 812 Araldite resin (polymerization at 60 °C for 15 h). Thin sections (60–80 nm) containing the cells were placed on grids and stained for 1 min each with 4% uranyl acetate (1:1, acetone/water) and 0.2% Reynold's lead citrate (water), air-dried, and imaged under an 80 kV JEM-1011 transmission electron microscope.

2.11. Pharmacokinetic studies

Healthy Sprague–Dawley rats (male, 200 ± 20 g) were used to examine the pharmacokinetics of PTX-PEG$_{1000}$@GNPs, and Taxol® was used as a reference. Rats were randomly divided into 2 groups ($n = 6$). Both Taxol® and PTX-PEG$_{1000}$@GNPs were intravenously administered through the tail vein with an equivalent dose of 7 mg/kg of PTX. Blood samples (0.5 mL) were collected from the plexus venous at various times (0.08, 0.17, 0.25, 0.5, 1, 2, 4, 6, 8, 12, 24 and 48 h) into heparinized tubes. The plasma samples were collected after immediate centrifugation at 1000× g for 10 min and stored at −20 °C until analysis. A 0.1 mL aliquot of plasma was mixed with 0.2 mL acetonitrile to extract the PTX, and plasma proteins were precipitated by vigorous vortexing. After centrifugation at 15,000× g for 10 min, the supernatant was analyzed by RP-HPLC described above.

2.12. In vivo antitumor efficacy

The in vivo antitumor efficacy of the PTX formulations was evaluated using animal tumor models after inoculation of hepatoma solidity (Heps). Healthy male ICR mice (20 ± 2 g) were purchased from the Zhejiang Experimental Animal Center (Certificate number: SCXK (Zhe) 20080033). Heps cells (Hepatoma solidity) were kindly provided by Nanjing University, and they were maintained as an ascites tumor in ICR mice. Heps cell suspensions containing 10^6 cells per 0.1 mL were implanted subcutaneously into the right axillary space. The tumor-bearing mice were subjected to antitumor activity studies after implantation. All the animals were pathogen free and allowed free access to food and water. The experiments were carried out in compliance with the National Institute of Health Guide for the Care and Use of Laboratory Animals.

To assess the antitumor activity of PTX-PEG$_{1000}$@GNPs, animals with a tumor volume of 200 mm^3 after Heps tumor inoculation were divided into three groups: saline, Taxol®, and PTX-PEG$_{1000}$@GNPs. Taxol® and PTX-PEG$_{1000}$@GNPs were diluted

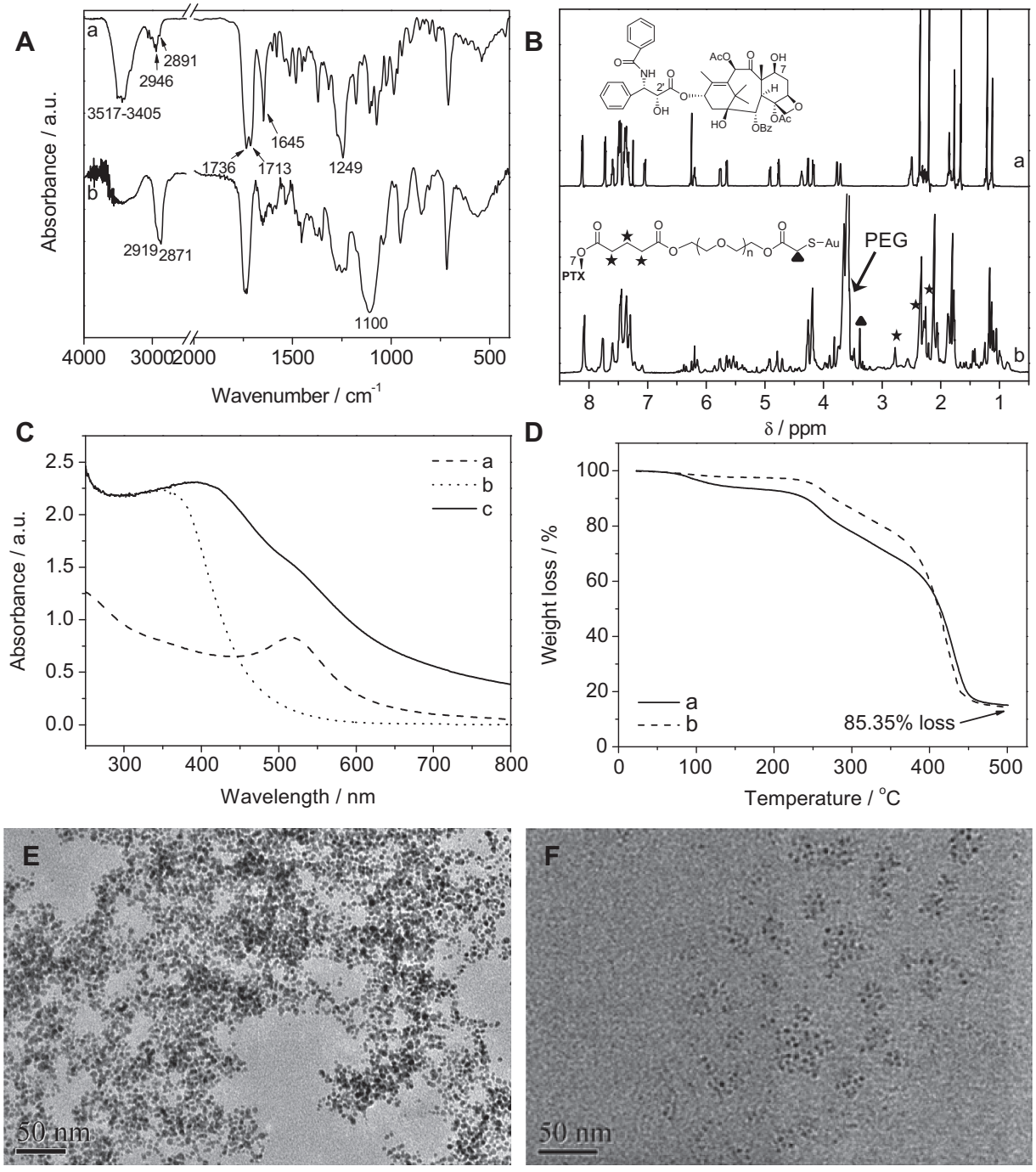

Fig. 2. Characterization of PTX-PEG@GNP conjugates with a PEG MW of 1000 Da (A) FT-IR spectra of PTX (curve a) and the PTX-PEG@GNP conjugate (curve b) in KBr. (B) ^{1}H NMR spectra of PTX (curve a) and the PTX-PEG@GNP conjugate (curve b) in $CDCl_3$. (C) UV–Vis spectra of (a) citrate-protected gold nanoparticles, (b) the PTX-PEG_{1000}-SH ligand, and (c) the PTX-PEG@GNP conjugate. (D) TGA measurement of the loss of organic material corresponding to the PTX-PEG@GNP conjugate (a) before and (b) after running a gel column. (E) and (F) TEM images of the citrate-protected gold nanoparticles and PTX-PEG@GNP conjugates, respectively.

in saline to a final PTX concentration of 1 mg/mL. Each treatment group was comprised of five tumor bearing mice. Tumor bearing mice were injected through the tail vein with 20 mg/kg of the indicated formulation in 2-day intervals. Tumor volume was calculated from the following equation: tumor volume (mm^3)=(length × $width^2$)/2. At the conclusion of the study, tumor tissues were excised, washed with saline and weighed.

2.13. Assay of PTX in blood, liver, and tumor tissues

ICR male mice (20 ± 2 g) with a tumor volume of 200 mm^3 after Heps tumor inoculation were randomly divided into two groups: (1) Taxol® and (2) PTX-PEG_{1000}@GNPs. Each group was injected intravenously through the tail vein with the indicated formulation at a dose of 20 mg/kg. After administration, blood was taken from the retro-orbital plexus at predetermined time points (0.5, 1, 4, 8, 12 and 24 h), and the samples were stored ($n = 5$ at each time point) at −20 °C until analysis. The mice were then sacrificed, and liver and tumor tissues were collected and stored at −20 °C until analysis.

The blood sample processing method is referred to that in the pharmacokinetic studies. Liver and tumor tissues were homogenized with 800 μL of saline, and 200 μL of the homogenate was deproteinized by 200 μL acetonitrile and centrifuged at 15,000 rpm for 10 min. Twenty microliters of the supernatant was analyzed by validated HPLC. The calibration curves of both tissue and blood displayed good linearity.

2.14. Histological analysis

The excised tumor tissues were weighed and fixed with 4% paraformaldehyde. The samples were processed and sectioned, and thin tissue sections were stained with hematoxylin and eosin (H and E) and Masson trichrome for histological observation (Olympus TH4-200, Olympus Optical Co., Ltd., Japan).

2.15. Statistical analysis

All the results are presented as the mean ± SD. The data were analyzed by one-way analysis of variance (ANOVA) with the appropriate Bonferroni correction to determine significant differences for multiple comparisons. $P < 0.05$ was considered to be statistically significant.

3. Results and discussion

3.1. Synthesis and solubility

The chemical reaction schemes used to synthesize the therapeutic ligands (PTX-PEG-SH) and the preparation of PTX-PEG@GNP conjugates are illustrated in the Supporting Information (Fig. S1). The therapeutic ligands consisted of a series of PEG derivatives of PTX, with PTX tagged on one end of PEG and a thiol group of mercaptoacetic acid on the other end. Glutaric acid was used as the connecting arm between PTX and the PEG molecule via an ester bond. To optimize the solubility of the GNP-based PTX conjugates and to regulate the size of the system, PTX-PEG-SH ligands with PEG MWs of 400, 600, and 1000 Da were synthesized. The PTX-PEG_{400}@GNPs were insoluble in water, but they easily dissolved in organic solvents such as chloroform and dimethyl sulfoxide. The water solubility of PEG_{600} was better than that of PTX-PEG_{400}@GNPs. However, the dissolution process was extremely slow, even with increased water volume and sonication. In contrast, the PTX-PEG_{1000}@GNPs dispersed easily in distilled water or phosphate buffer solution (PBS) to produce a clear, light orange solution. The solubility of this conjugate reached 512 mg/mL. Thus, the PTX-PEG_{1000}@GNP conjugate was selected for further studies.

3.2. Characterization

The chemical structure of the organic outer layer of the PTX-PEG@GNP conjugate was characterized via FT-IR and NMR methods. The FT-IR spectra of PTX and the PTX-PEG@GNP conjugate are shown in Fig. 2A. For paclitaxel (curve a), the FT-IR spectrum was consistent with a previous report [33]. The infrared peaks of the N–H stretching vibrations were located at 3517–3405 cm^{-1}, and CH_2 asymmetric and symmetric stretching vibrations were located at 2946 and 2891 cm^{-1}. The peaks situated at 1736 and 1713 cm^{-1} are representative of C=O stretching vibrations from the ester groups. The amide bond was located near 1645 cm^{-1}. Absorption at 1608 cm^{-1} and 1589 cm^{-1} were identified to be aromatic bonds. An ester bond stretching vibration was situated at 1249 cm^{-1}. The FT-IR spectrum of the PTX-PEG_{1000}@GNP conjugate contains the characteristic infrared signals of both PTX and PEG, typical of CH_2 stretching vibrations at 2919 cm^{-1} and the backbone C–O stretching at 1100 cm^{-1} of PEG. In addition, the absorption peaks in the infrared spectroscopy of PTX-PEG@GNP conjugate were broader compared to PTX and the therapeutic ligand (PTX-PEG-SH, not shown). Taken together, these data confirm the successful conjugation of ligands on the surface of gold nanoparticles via the S–Au bond [34].

The proton NMR spectra for the PTX (curve a) and the as-prepared PTX-PEG@GNP conjugate (curve b) in $CDCl_3$ are shown in Fig. 2B. Compared with the proton NMR signals of PTX, the ^1H NMR spectrum of the PTX-PEG@GNP conjugate exhibited a new, broad resonance at 3.7 ppm that corresponds to the protons of PEG connected at the C-7 position of PTX, and the characteristic peaks of PTX were also observed. This spectrum revealed the existence of PEG and PTX in the conjugate, and additional chemical shifts at ca. 2.8, 2.4, and 2.3 ppm (marked with stars in Fig. 2B) can be attributed to protons in the glutaric acid spacer. This result demonstrated that the glutaric acid spacer was successfully linked between the PEG and PTX molecules. Furthermore, the signal at 3.4 ppm (marked with a triangle) can be attributed to the proton in thioglycolic acid, confirming the successful derivation of the thiol group on the distal end of the therapeutic ligand (PTX-PEG_{1000}-SH here).

UV–Vis spectra of citrate-protected gold nanoparticles, PTX-PEG_{1000}-SH ligand, and PTX-PEG_{1000}@GNPs are shown in Fig. 2C. The citrate-stabilized gold nanoparticles display a characteristic UV–Vis absorption spectrum, with a surface-localized plasmon resonance band at 516 nm (dashed curve a), which reflects the existence of gold nanoparticles with diameters of approximately 3–4 nm. The maximum absorption of the PTX-PEG_{1000}-SH ligand appears at about 349 nm (dotted curve b). Regarding the PTX-PEG_{1000}@GNP conjugate (the solid curve c), the UV–Vis spectrum displayed a broad band from 290 to 700 nm, which covers the UV–Vis absorption of both gold nanoparticles and therapeutic ligands. This phenomenon could be attributed to the additive characteristics of the chromophores and further manifestation of successful conjugation of therapeutic ligand on the surface of gold nanoparticles via the S–Au bond.

To determine the PTX loading capacity in the conjugates, TGA was carried out to evaluate organic loss from the PTX-PEG_{1000}@GNP conjugate sample before and after it was run on a gel column. The TGA curves shown in Fig. 2D demonstrate that the composition of the PTX-PEG_{1000}@GNP conjugate was 85.35% organic and 14.65% metallic gold. Because the molar mass of PTX and PTX-PEG_{1000}-S- are 853.92 g/mol and 2023 g/mol, respectively, the DLC of conjugate is calculated to be 36.0%. This value is much higher than that of previously reported PTX-conjugated gold nanoparticles [2,4,23,24]. Moreover, according to the TGA result, the solubility of the PTX-PEG_{1000}@GNP conjugate (512 mg/mL) is equivalent to 184 mg/mL PTX in dispersion. Compared to the parent paclitaxel molecule (0.4 μg/mL) [25], the hydrophilicity of the PTX-PEG_{1000}@GNP conjugate was 4.6×10^5 times greater. This result is 73.6-fold higher than the *N*-octyl-*O*-sulfate chitosan micelles encapsulated paclitaxel (2.5 mg/mL) described in our previous report [27]. Thus, the strong S–Au interaction between PTX-PEG-SH and the gold nanoparticle made ligand exchange of the citrate salt from the gold surface simple. The increased length and the flexibility of the PEG

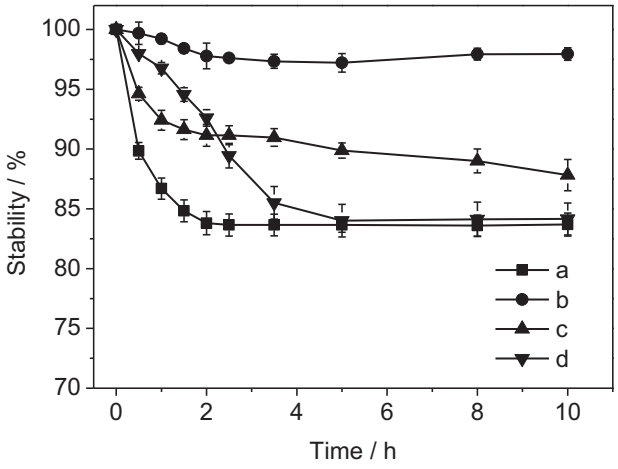

Fig. 3. Dispersion stability of the PTX-PEG_{1000}@GNP conjugate as a function of time in the following environments: 0.03 M PBS at pH 7.4 (curve a), 0.03 M PBS at pH 5.5 (curve b), 0.2 M PBS at pH 7.4 (curve c), and 0.03 M PBS with 2% serum (curve d).

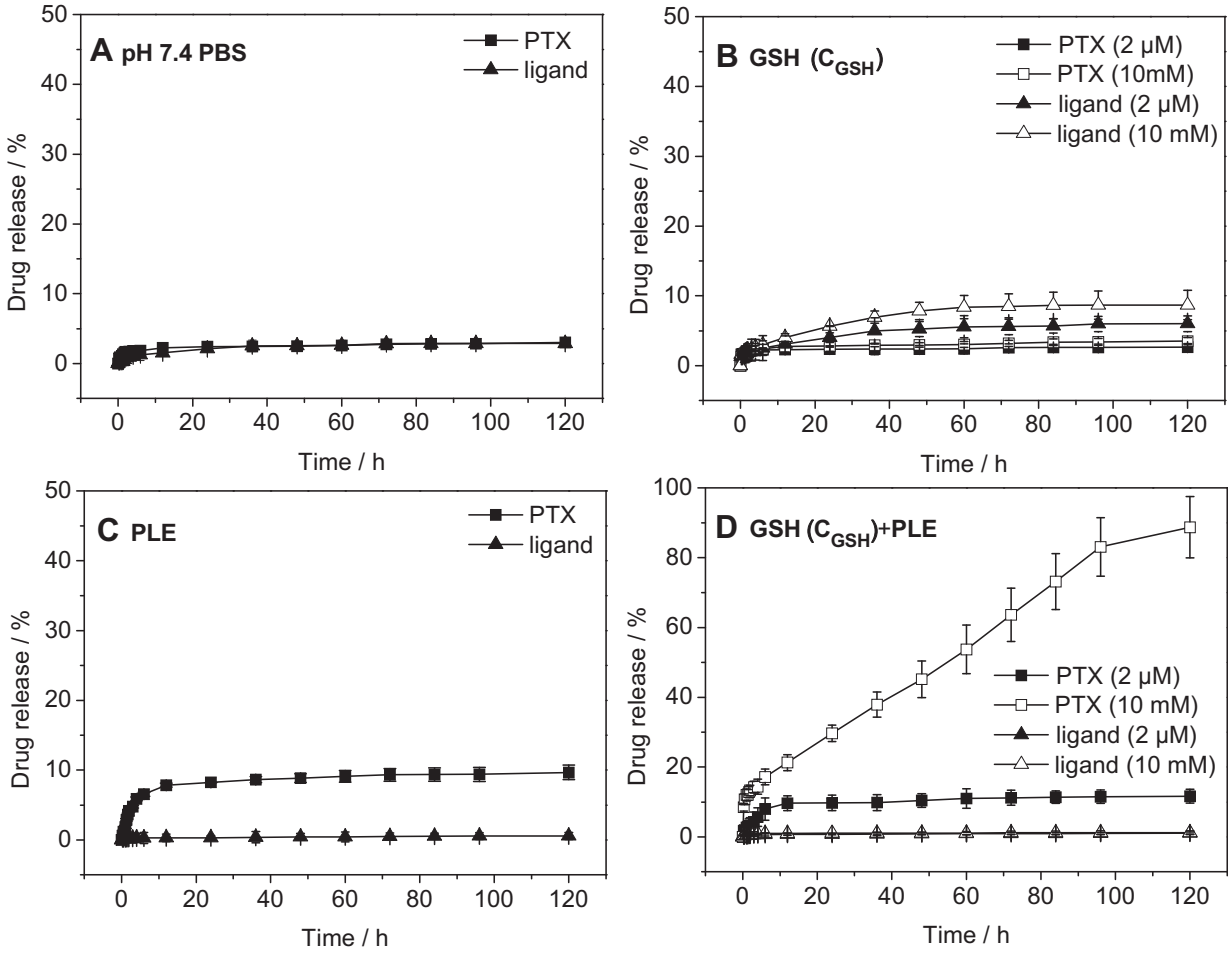

Fig. 4. Drug release profiles of paclitaxel and the therapeutic ligand from the PTX-PEG_{1000}@GNP conjugate (A) in the release media (PBS at pH 7.4), (B) release media with intracellular and extracellular concentration of GSH (10 mM and 2 μM, respectively), (C) release media containing pig liver esterase (20 units), and (D) the combination of release media with different concentrations of GSH (B) and in the presence of pig liver esterase ($n = 3$, mean ± SD).

linker not only bestowed the conjugate with high water solubility but also offered a broader space that reduced the steric hindrance between PTX molecules. In addition, the amount of weight loss before and after running a gel column was similar at a temperature of 500 °C, confirming the effective separation of the ligand from the conjugate using a dialysis method. Therefore, the conjugate sample used for in vitro and in vivo studies was purified using only dialysis.

To investigate the size and morphology of PTX-PEG_{1000}@GNPs, the citrate-protected gold nanoparticles and PTX-PEG_{1000}@GNP dispersion were observed by TEM (Fig. 2 E and F). The citrate-protected gold nanoparticles are spherical, with a diameter of 3.35 ± 0.38 nm, as determined by averaging the size of 100 particles in the image (Fig. 2E), and the particles are not well dispersed. After surface modification of the as-synthesized therapeutic ligand (Fig. 2F), the shape and size of the gold core remained unchanged. The interparticle distance increased compared with that of the citrate-protected gold nanoparticles, and the edges of the particles were vague, which was due to the successful conjugation of organic ligands to the gold nanoparticle surface. In addition, the conjugates deposited on the grid were dispersed in clusters composed of 8–12 particles, likely due to hydrophobic interactions between PTX molecules on the outer layer of the conjugates. This result was consistent with the DLS data, which indicated that the average diameter of the conjugate was approximately 155.0 ± 24.2 nm. This value is considerately larger than the size of a one-particle conjugate, as determined by TEM (Fig. 2F). Moreover, the zeta potential value changed from −32.27 ± 1.66 mV (the citrate-protected gold nanoparticles) to −14.38 ± 1.89 mV (the PTX-PEG_{1000}@GNP conjugate) after surface modification of the therapeutic ligand, confirming that the citrate salt was replaced from the gold surface of nanoparticles via the ligand exchange reaction.

3.3. Stability studies

To evaluate the stability of the gold-drug conjugates in different environments that are known to immediately induce the aggregation of unmodified gold particles, the UV–Vis absorption intensity at 520 nm was measured as a function of time (Fig. 3). The decay of the optical absorbance of the particle suspension at 520 nm was negligible for the PTX-PEG_{1000}@GNP conjugate (curve b) in 0.03 M PBS at a pH of 5.5, suggesting that the PTX-PEG_{1000}@GNP conjugate is highly stable in buffers with low pH values. This characteristic is likely due to the protonation of carbonyl groups in the chemical structure of PTX and oxide atoms in PEG chain. The relative absorbance of each group at 12 h was no less than 82.5% of the gold conjugates at 0 h, indicating that the conjugates are stable in buffers with neutral pH values (pH 7.4; curve a), elevated salt concentrations (0.2 M PBS, pH 7.4; curve c), and in the presence of serum (curve d). The high stability of the

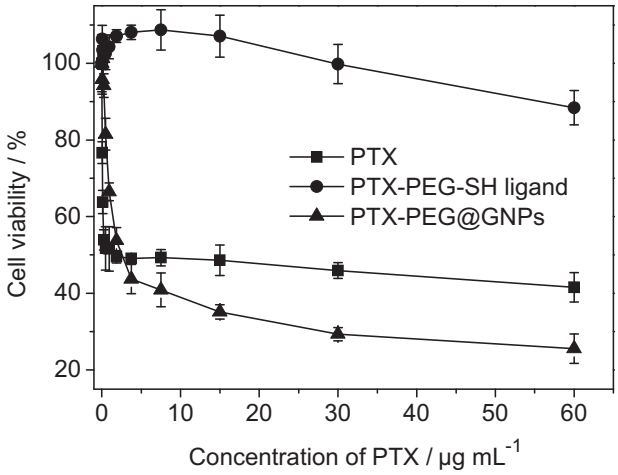

Fig. 5. In vitro MTT assays to measure the cytotoxicity of the PTX, PTX-PEG_{1000}-SH ligand and PTX-PEG_{1000}@GNPs with varying paclitaxel concentrations for 48 h in HepG2 cells.

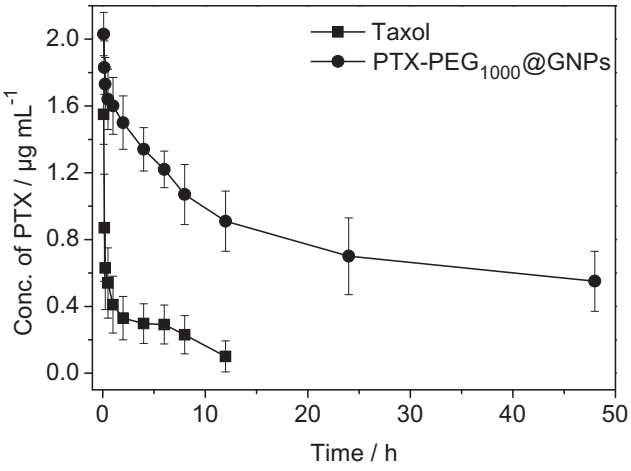

Fig. 7. Plasma concentration–time profiles of PTX in rats following intravenous administration of Taxol® and PTX-PEG_{1000}@GNPs (7 mg/kg) (mean ± SD, $n = 6$).

conjugates in vitro could be due to the covalent linkage of all the components in the system.

3.4. In vitro drug release

To achieve selective drug release inside tumor cells, the structure and composition of the GNP-based conjugates were designed to achieve two goals: therapeutic ligand exchange in response to high concentration of GSH inside tumor cells and cutting of the ester bond between PTX and PEG spacer by esterase (Fig. 1A). Thus, in vitro drug release studies of PTX-PEG_{1000}@GNP conjugates were systematically investigated under the following conditions: (1) the physiological environment (PBS, pH 7.4), (2) the intracellular and extracellular GSH concentration (10 mM and 2 μM, respectively), (3) the absence and presence of PLE, and (4) the combination condition of GSH (either 2 μM or 10 mM) and PLE, which simulates the in vivo environments outside and inside cells, respectively. The drug release behaviors of PTX-PEG_{1000}@GNPs, including the release of the PTX-PEG_{1000}-SH ligand and free PTX, were detected using HPLC, and the profiles are shown in Fig. 4.

The in vitro drug release profiles shown in Fig. 4 provide several clues that reveal the potential characteristics of PTX liberated from

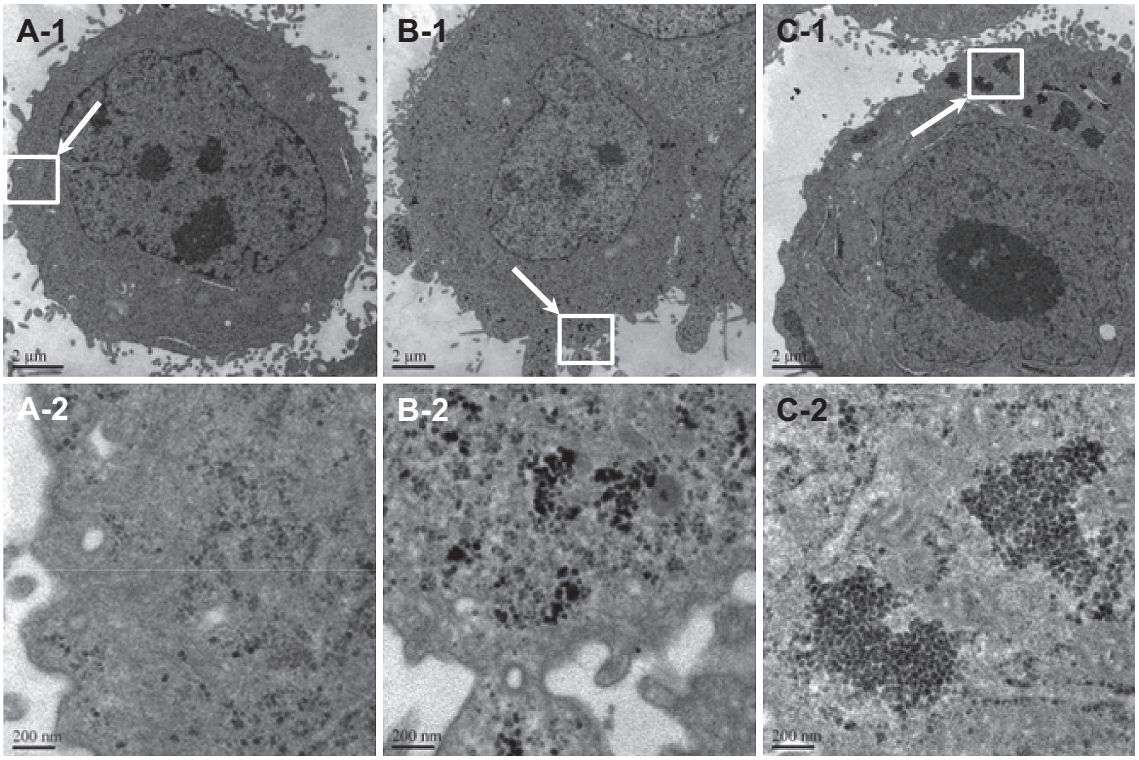

Fig. 6. Transmission electron microscopy of HepG2 cells under the following conditions: cells cultured with drug-free medium (A), or with PTX-PEG_{1000}@GNPs for 4 h (B) and 8 h (C).

Table 1
Pharmacokinetic parameters of Taxol® and PTX-PEG_{1000}@GNPs after i.v. administration.

	Taxol®	PTX-PEG_{1000}@GNPs
$AUC_{0-\tau}$ (h mg/L)[a]	3.36 ± 1.23	39.51 ± 8.79*
$t_{1/2}$ (h)[b]	28.66 ± 22.82	33.81 ± 20.89
MRT (h)[c]	4.27 ± 0.91	19.01 ± 1.71*
CL (L/h/kg)[d]	0.76 ± ± 0.45	0.13 ± ± 0.07
V_d (L/kg)[e]	21.83 ± 12.53	5.04 ± 0.42*

Data represent mean ± SD, $n = 6$.
*$P < 0.05$ compared with Taxol®.
[a] $AUC_{0-\tau}$, area under the plasma concentration–time curve.
[b] $t_{1/2}$, plasma half-life.
[c] MRT, mean residence time.
[d] CL, total body clearance.
[e] V_d, apparent volume of distribution.

the conjugates prepared in this work. First, Fig. 4A shows the drug release profiles of free paclitaxel and PTX-PEG_{1000}-SH ligand in PBS (pH 7.4) as a function of release time. The release of free paclitaxel and the therapeutic ligand did not exceed 3% of the total drug content in the conjugates at 120 h, indicating that the conjugates are highly stable in an aqueous solution at physiological pH.

The release profiles of the conjugates at extracellular and intracellular GSH concentration (2 μM and 10 mM, respectively) are shown in Fig. 4B. The mechanism of GSH-induced drug release from the conjugates was related to the thiol group exchange reaction, in which GSH functions as a reducing agent to exchange the therapeutic ligands from the surface of the gold. These data revel that the drug was liberated from the conjugates in the form of ligands, especially in the release media with intracellular GSH levels (e.g., 10 mM). The cumulative drug release peaked after 60 h at ca. 8.68%, indicating that the release velocity of the ligands was slow and controlled by the GSH concentration-dependent ligand exchange rate.

The drug release curves in the release media containing PLE are displayed in Fig. 4C. Because mammalian esterases are widely distribute throughout the plasma, many organs, and tissues [35,36], PLE was used to study the stability of the conjugates and drug release in the simulated body environment. In this condition, instead of ligands, free paclitaxel was dissociated from the conjugate at a relatively rapid speed within 12 h. We found that the cumulative percentage of paclitaxel release in the presence of PLE did not exceed 10% (9.67% at 120 h), indicating that the conjugate could remain stable in circulation for long periods of time in vivo.

Therefore, the percentage of drug release from conjugate is quite low in response to either high GSH concentrations or esterase (not more than 10% for the cumulative value in 120 h). These results can be attributed to enhanced drug loading on the surface of the gold nanoparticles, which forms an organic shell with high density. The unique structure of the conjugates hinders the approach and infiltration of both small molecules, such as GSH, and biological macromolecules, such as esterases. Therefore, we believe that drug release from the conjugate in vivo will proceed in a synergistic manner and was demonstrated by the in vitro release study in the combination condition. As shown in Fig. 4D, the paclitaxel molecule was almost completely released from the conjugate in PBS at pH 7.4 with 10 mM intracellular GSH plus PLE, and the GSH ligand exchange reaction was the rate-limiting step. These data suggest the following: (1) the drug will only be released form the particle surface when the conjugate enters into the cancer cell; (2) liberation of the therapeutic ligand from the surface of gold nanoparticles would eliminate the steric hindrance in the organic outer layer and accelerate the hydrolysis rate of esterase, releasing free paclitaxel; and (3) sustained release behavior over 120 h can be achieved. Therefore, the chemical structure of conjugates we designed in this work can achieve targeted drug release in a synergistic manner in cancer cells. The drug release mechanism is dependent on high GSH concentration-dependent ligand exchange and sterically influenced enzymatic hydrolysis reactions. The combination of these two drug release mechanisms permits the rapid transformation of PTX-PEG_{1000}@GNP conjugates into free PTX inside tumor cells, which we expect will improve tumor cell inhibition. Subsequently, we performed in vitro cytotoxicity assays to further identify the intracellular targeting drug release of the conjugates.

3.5. Cytotoxicity assays, cellular uptake, and intracellular distribution

Fig. 5 shows the viability of HepG2 cells after treatment with the distinct paclitaxel formulations investigated in this study. Compared to free paclitaxel, the PTX-PEG_{1000}-SH ligand was not cytotoxic toward HepG2 cells within the measured concentrations. This phenomenon is likely due to the reduced biological activity and decreased cellular uptake of the PTX-PEG_{1000}-SH ligand because of the covalent modification and shield effect of the PEG molecule. We also observed that the cytotoxicity of PTX-PEG_{1000}@GNPs with the same dose of PTX was slightly lower than that of free PTX at low concentrations (from 0 to 2.5 μg/mL PTX) and that the mean concentration of paclitaxel that caused 50% inhibition of cell viability (IC_{50}) was increased from 1.86 μg/mL for free paclitaxel to 2.39 μg PTX equiv./mL for PTX-PEG_{1000}@GNPs. However, PTX-PEG_{1000}@GNPs showed significantly higher cytotoxicity than free paclitaxel when concentrations were increased from 2.5 to 60 μg/mL. Because we observed that the citrate-protected GNPs were not cytotoxic toward HepG2 cells (data not shown), the cytotoxicity of PTX-PEG_{1000}@GNPs toward HepG2 cells can be attributed to the release of free PTX molecules from the conjugates. Therefore, the high cytotoxicity of drug-loaded nanoparticles was due to increased cellular uptake via the endocytosis, and intracellular paclitaxel was released via the synergistic mechanism we described above.

To investigate the cellular uptake of PTX-conjugated GNPs and their distribution inside tumor cells, HepG2 cells were incubated with the PTX-PEG_{1000}@GNP formulation (equivalent to 2 μg/mL PTX) for 4 h and 8 h and evaluated by TEM. As shown in Fig. 6 (B-1 and B-2), PTX-PEG_{1000}@GNP conjugates were present in the cytoplasm of HepG2 cells after 4 h of incubation, and the particles tend to stick to each other due to the hydrophobic interactions of between the PTX molecules located on the particle surface. Fig. 6 C-1 and C-2 show that more nanoparticles were localized in the cytoplasm after 8 h of incubation compared to 4 h, and they were well dispersed and had more uniform interparticle distance, indicating that free PTX was released gradually from the nanoparticle after 8 h of incubation and the protector of GNPs changed into GSH molecules. These results confirmed that the particle endocytosis-induced drug accumulation in tumor cells is responsible for the differences between the therapeutic ligand and drug-conjugated GNPs in the cytotoxicity studies.

3.6. Pharmacokinetic studies

After intravenous administration of Taxol® and PTX-gold conjugates in rats, we characterized the plasma concentration–time profiles of PTX (Fig. 7). The pharmacokinetic parameters of PTX in the two formulations are presented in Table 1. As shown in Fig. 7, PTX-PEG_{1000}@GNPs produced a higher plasma concentration of PTX than Taxol® from 5 min to 48 h and the plasma PTX concentration after Taxol® administration was much lower than that obtained with PTX-PEG_{1000}@GNPs. For PTX-PEG_{1000}@GNPs, the area under the plasma concentration–time curve ($AUC_{0-\infty}$) was

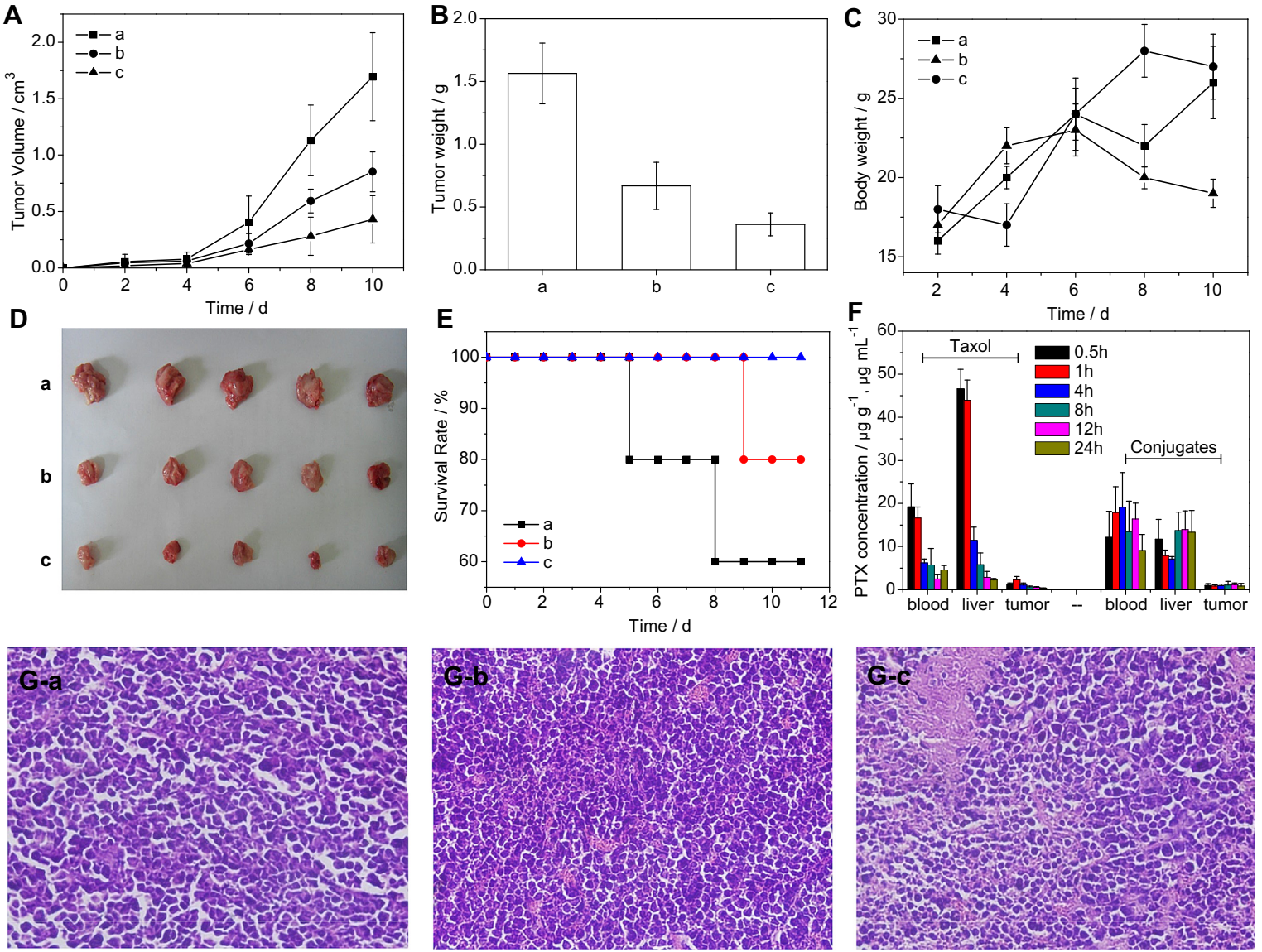

Fig. 8. In vivo antitumor efficacy of (a) saline, (b) Taxol®, and (c) PTX-PEG$_{1000}$@GNPs in Heps tumor xenograft ICR mouse models: (A) tumor volume changes, (B) tumor tissue weight, (C) body weight changes during the 10-day treatment, and (D) images of the tumor tissues excised from mice on day 10. (E) Survival rates of the three groups of tumor-bearing mice. (F) PTX concentrations in the blood and tumor tissues of tumor-bearing mice after i.v. administration of Taxol® and PTX-PEG$_{1000}$@GNP conjugates at 0.5, 1, 4, 8, 12, and 24 h. (G) H&E stained tumor tissue sections from control and test groups at 10 days post-injection. Each point in (A–C, E, and F) represents the mean ± SD ($n = 5$).

39.51 ± 8.79 h mg/L, which was approximately 12-fold higher than Taxol® (3.36 ± 1.23 h mg/L), and the corresponding total body clearance (CL) was 0.13 ± 0.07 L/h/kg, which was 6-fold lower than Taxol® (0.76 ± 0.45 L/h/kg). These data suggest that the conjugate groups displayed slower elimination of PTX, longer plasma half-life ($t_{1/2}$), and longer mean residence time (MRT) compared to Taxol®, confirming the longer circulation characteristics of PTX-PEG_{1000}@GNPs in blood.

3.7. Antitumor activity in vivo

Antitumor efficacy was evaluated in ICR mice bearing Heps tumors. Changes in tumor volume, final tumor weight, tumor images, and the body weight of mice treated with saline, Taxol®, and PTX-PEG_{1000}@GNPs are presented in Fig. 8 A–D. Tumor growth was significantly suppressed in the group treated with PTX-PEG_{1000}@GNPs compared to saline and Taxol®. Although the mice in the PTX-PEG_{1000}@GNP group had the smallest tumor size and tumor weight, their body weight (27.0 ± 2.0 g) was the heaviest and the increment of body weight (9.0 g) also exceeded that of the other groups. These results are consistent with improved quality of life in mice treated with the conjugate.

We observed significant differences in the survival rates of the PTX-PEG_{1000}@GNP- and saline-treated groups (Fig. 8 E). No mice died in the PTX-PEG_{1000}@GNP-treated group ($n = 5$) after 10 days, whereas the survival rates of the saline and Taxol® groups were only 60% and 80%, respectively. Thus, treatment with PTX-PEG_{1000}@GNPs not only effectively prolongs life, but it also shows reduced systemic toxicity in vivo.

We believe that the excellent therapeutic efficacy of PTX-PEG_{1000}@GNPs (100% survival rate after 10 days) is due to its long circulation and the successful passive tumor targeting of the conjugates in tumor tissues. The PTX concentration in the blood, liver, and tumor tissues of tumor bearing mice treated with Taxol® and PTX-PEG_{1000}@GNP conjugates were shown in Fig. 8F. It is found that the PTX concentration in the blood, liver, and tumor decreased gradually with time going. However, the PTX concentration in blood treated with PTX-PEG_{1000}@GNP conjugates kept relatively high PTX level (2-fold higher than that treated with Taxol®) even after 24 h administration. This result provides additional evidence for the high stability and sustained drug release of the conjugates observed in in vitro drug release assays. The high drug concentration in liver indicates the passive target capability and accumulation of conjugate in liver, which allows it a promising nanoprodrug for the treatment of liver cancer. In addition, the PTX concentration in the tumor tissues from the PTX-PEG_{1000}@GNP group was higher, and it was eliminated more slowly than was observed for the Taxol® group. The PTX level in the tumor tissues from conjugate-treated mice at 24 h (0.84 ± 0.61 μg/g) was 2.6-fold higher than that of Taxol® at 24 h (0.32 ± 0.09 μg/g). This result indicates that the high stability- and long circulation-induced passive tumor targeting characteristics of the conjugate promote intratumoral accumulation of the system, which allows for the release of PTX within target tumor cells via a double simultaneous stimulation.

To determine the extent of tumor damage in response to concentrated distribution of the conjugate and the high level of PTX released from it, we performed histological examination of H&E stained tumor tissue sections at 10 day post-injection (Fig. 8G). Almost no damage was observed in tumors from the saline-treated group (Fig. 8G-a), but significant necrosis was present in both the Taxol® and PTX-PEG_{1000}@GNP-treated groups. Moreover, larger necrosis regions were observed in tumors from the PTX-PEG_{1000}@GNP group (Fig. 8G-c) compared to the Taxol® group (Fig. 8G-b). These data further confirmed the therapeutic effect of the nanoprodrug. Therefore, the enhanced accumulation and controlled drug release in tumor tissues ensured that higher amounts of PTX were delivered to tumor cells, resulting in increased therapeutic efficacy and antitumor efficiency.

4. Conclusions

To improve the overall performance of paclitaxel-conjugated gold nanoparticles, we synthesized a series of polyethylene glycol derivatives with paclitaxel on one end and a thiol group on the other end. The resulting hybrid structure of the nanoprodrug system has superior properties, including enhanced water solubility, drug loading, and targeted drug release inside tumor cells, resulting in enhanced tumor cell killing ability in vitro and tumor therapeutic efficacy in vivo. The nanoprodrug system constructed in this work overcomes some of the problems associated with the practical application of paclitaxel and improves upon the advantages of nanoparticles as a drug delivery system. The advantages of this system, including superior biological activity and therapeutic efficiency, indicate that this system is a promising approach for in vivo tumor therapy.

Acknowledgment

This work was supported by the Natural Science Foundation of China (30900337), the Doctoral Fund of Ministry of Education of China (20090096120001), the China Postdoctoral Science Foundation (2008440155, 201003566), the Fundamental Research Funds for the Central Universities (JKQ2009026, JKP2011008), the Qing Lan Project, the Program for New Century Excellent Talents in University (NCET-10-0816), and the Open Project Program of MOE Key Laboratory of Drug Quality Control and Pharmacovigilance (MKLDP2013MS04).

Appendix A. Supplementary data

Supplementary data related to this article can be found at http://dx.doi.org/10.1016/j.biomaterials.2013.09.008.

References

[1] Zhang Z, Mei L, Feng SS. Paclitaxel drug delivery systems. Expert Opin Drug Deliv 2013;10:325–40.
[2] Paciotti GF, Myer L, Weinreich D, Goia D, Pavel N, McLaughlin RE, et al. Colloidal gold: a novel nanoparticle vector for tumor directed drug delivery. Drug Del 2004;11:169–83.
[3] Dykmana L, Khlebtsov N. Gold nanoparticles in biomedical applications: recent advances and perspectives. Chem Soc Rev 2012;41:2256–82.
[4] Paciotti GF, Kingston DGI, Tamarkin L. Colloidal gold nanoparticles: a novel nanoparticle platform for developing multifunctional tumor-targeted drug delivery vectors. Drug Develop Res 2006;67:47–54.
[5] Tom RT, Suryanarayanan V, Reddy PG, Baskaran S, Pradeep T. Ciprofloxacin-protected gold nanoparticles. Langmuir 2004;20:1909–14.
[6] Zhang X, Chibli H, Mielke R, Nadeau J. Ultrasmall gold-doxorubicin conjugates rapidly kill apoptosis-resistant cancer cells. Bioconjugate Chem 2011;22:235–43.
[7] Aryal S, Grailer JJ, Pilla S, Steeber DA, Gong S. Doxorubicin conjugated gold nanoparticles as water-soluble and pH-responsive anticancer drug nanocarriers. J Mater Chem 2009;19:7879–84.
[8] Wang F, Wang YC, Dou S, Xiong MH, Sun TM, Wang J. Doxorubicin-tethered responsive gold nanoparticles facilitate intracellular drug delivery for overcoming multidrug resistance in cancer cells. ACS Nano 2011;5:3679–92.
[9] Chen H, Li B, Ren X, Li S, Ma Y, Cui S, et al. Multifunctional near-infrared-emitting nano-conjugates based on gold clusters for tumor imaging and therapy. Biomaterials 2012;33:8461–76.
[10] Manju S, Sreenivasan K. Gold nanoparticles generated and stabilized by water soluble curcumin–polymer conjugate: blood compatibility evaluation and targeted drug delivery onto cancer cells. J Colloid Inter Sci 2012;368:144–51.

[11] Joshi P, Chakraborty S, Dey S, Shanker V, Ansari ZA, Singh SP, et al. Binding of chloroquine–conjugated gold nanoparticles with bovine serum albumin. J Colloid Inter Sci 2001;355:402–9.
[12] Fleigea E, Quadirb MA, Haag R. Stimuli-responsive polymeric nanocarriers for the controlled transport of active compounds: concepts and applications. Adv Drug Del Rev 2012;64:866–84.
[13] Cline EN, Li MH, Choi SK, Herbstman JF, Kaul N, Meyhöfer E, et al. Paclitaxel-conjugated PAMAM dendrimers adversely affect microtubule structure through two independent modes of action. Biomacromolecules 2013;14:654–64.
[14] Danhier F, Lecouturie N, Vroman B, Jérôme C, Marchand-Brynaert J, Feron O, et al. Paclitaxel-loaded PEGylated PLGA-based nanoparticles: In vitro and in vivo evaluation. J Control Release 2009;133:11–7.
[15] Farokhzad OC, Cheng J, Teply BA, Sherifi I, Jon S, Kantoff PW, et al. Targeted nanoparticle-aptamer bioconjugates for cancer chemotherapy in vivo. Proc Natl Acad Sci U S A 2006;103:6315–20.
[16] Gref R, Minamitake Y, Peracchia MT, Trubetskoy V, Torchilin V, Langer R. Biodegradable long-circulating polymeric nanospheres. Science 1994;263:1600–3.
[17] Chithrani BD, Chan WCW. Elucidating the mechanism of cellular uptake and removal of protein-coated gold nanoparticles of different sizes and shapes. Nano Lett 2007;7:1542–50.
[18] Cheng JY, Wang DL, Xi JF, Au L, Siekkinen A, Warsen A, et al. Immuno gold nanocages with tailored optical properties for targeted photothermal destruction of cancer cells. Nano Lett 2007;7:1318–22.
[19] Maeda H. The enhanced permeability and retention (EPR) effect in tumor vasculature: the key role of tumor-selective macromolecular drug targeting. Advan Enzyme Regul 2001;41:189–207.
[20] Duncan R, Sat YN. Tumour targeting by enhanced permeability and retention (EPR) effect. Ann Oncol 1998;9(Suppl. 2):39–50.
[21] Yue T, Zhang X. Cooperative effect in receptor-mediated endocytosis of multiple nanoparticles. ACS Nano 2012;6:3196–205.
[22] Hong R, Han G, Fernández JM, Kim BJ, Forbes NS, Rotello VM. Glutathione-mediated delivery and release using monolayer protected nanoparticle carriers. J Am Chem Soc 2006;128:1078–9.
[23] Gibson JD, Khanal BP, Zubarev ER. Paclitaxel-functionalized gold nanoparticles. J Am Chem Soc 2007;129:11653–61.
[24] Zhang XQ, Xu X, Lam R, Giljohann D, Ho D, Mirkin CA. Strategy for increasing drug solubility and efficacy through covalent attachment to polyvalent DNA-nanoparticle conjugates. ACS Nano 2011;5:6962–70.
[25] Skwarczynski M, Hayashi Y, Kiso Y. Paclitaxel prodrugs: toward smarter delivery of anticancer agents. J Med Chem 2006;49:7253–69.
[26] Hwu JR, Lin YS, Josephrajan T, Hsu MH, Cheng FY, Yeh CS, et al. Targeted paclitaxel by conjugation to iron oxide and gold nanoparticles. J Am Chem Soc 2009;131:66–8.
[27] Mo R, Jin X, Li N, Ju C, Sun M, Zhang C, et al. The mechanism of enhancement on oral absorption of paclitaxel by N-octyl-O-sulfate chitosan micelles. Biomaterials 2011;32:4609–20.
[28] Li Y, Xu X, Shen Y, Qian C, Lu F, Guo S. Preparation and evaluation of copolymeric micelles with high paclitaxel contents and sustained drug release. Colloid Surf A 2013;429:12–8.
[29] Kataoka K, Harada A, Nagasaki Y. Block copolymer micelles for drug delivery: design, characterization and biological significance. Adv Drug Delivery Rev 2001;47:113–31.
[30] Ding Y, Xia XH, Zhai HS. Reversible assembly and disassembly of gold nanoparticles directed by a zwitterionic polymer. Chem Eur J 2007;13:4197–302.
[31] Ding Y, Gu G, Xia XH. Cysteine-grafted chitosan-mediated gold nanoparticle assembly: from nanochains to microcubes. J Mater Chem 2009;19:795–9.
[32] Mathew AE, Mejillano MR, Nath JP, Himes RH, Stella VJ. Synthesis and evaluation of some water-soluble prodrugs and derivatives of taxol with antitumor activity. J Med Chem 1992;35:145–51.
[33] Garea SA, Ghebaur A. FT-IR spectroscopy and thermogravimetrical characterization of prodrugs based on different dendritic polymers and antitumoral drug. Mater Plast 2012;49:1–4.
[34] Ding Y, Xia XH, Zhang C. Synthesis of metallic nanoparticles protected with N, N, N-trimethyl chitosan chloride via a relatively weak affinity. Nanotechnology 2006;17:4156–62.
[35] Maxwell DM, Brecht KM, O'Neill BL. The effect of carboxylesterase inhibition on interspecies differences in soman toxicity. Toxicol Lett 1987;39:35–42.
[36] Maxwell DM, Lenx DF, Groff WA, Kaminskis A, Froehlich HL. The effects of blood flow and detoxification on in vivo cholinesterase inhibition by soman in rats. Toxicol Appl Pharmacol 1987;88:66–76.